Journal of Solid State Chemistry **162,** 103–112 (2001)
doi: 10.1006/jssc.2001.9361, available online at http://www.idealibrary.com on IDEAL®

Influence of the Metal–Metal Sigma Bonding on the Structures and Physical Properties of the Hexagonal Perovskite-Type Sulfides $Sr_{9/8}TiS_3$, $Sr_{8/7}TiS_3$, and $Sr_{8/7}[Ti_{6/7}Fe_{1/7}]S_3$

O. Gourdon, E. Jeanneau, M. Evain, S. Jobic,[1] and R. Brec

Institut des Matériaux Jean Rouxel, Laboratoire de Chimie des Solides, Université de Nantes, 44322 Nantes Cedex 3, France

and

H.-J. Koo and M.-H. Whangbo[1]

Department of Chemistry, North Carolina State University, Raleigh, North Carolina 27695-8204

Received May 15, 2001; in revised form August 3, 2001; accepted August 16, 2001

The structural and electronic consequences of the metal–metal sigma bonding in the hexagonal perovskite sulfides were examined by calculating the electronic band structures of $Sr_{9/8}TiS_3$ and $Sr_{8/7}TiS_3$, by synthesizing $Sr_{8/7}[Ti_{6/7}Fe_{1/7}]S_3$ and characterizing its crystal structure, and by measuring the magnetic susceptibilities of $Sr_{9/8}TiS_3$, $Sr_{8/7}TiS_3$, and $Sr_{8/7}[Ti_{6/7}Fe_{1/7}]S_3$. The $(TiS_3)_\infty$ chains of $Sr_{9/8}TiS_3$ and $Sr_{8/7}TiS_3$ contain oligomer units $(Oh)_n$ ($n = 4, 5$) made up of face-sharing TiS_6 octahedra (Oh). Given the $(TiS_3)_\infty$ chains aligned along the z direction, the only occupied d-block levels of each $(TiS_3)_\infty$ chain are the most sigma bonding level of each $(Oh)_n$ oligomer, which is constructed from its n z^2 orbitals. This "n-orbital two-electron" metal–metal sigma bonding controls the d-orbital density distribution and the Ti–Ti distances of the $(Oh)_n$ oligomers and is ultimately responsible for the semiconducting property of $Sr_{9/8}TiS_3$, $Sr_{8/7}TiS_3$, and $Sr_{8/7}[Ti_{6/7}Fe_{1/7}]S_3$. The $Sr_{8/7}[Ti_{6/7}Fe_{1/7}]S_3$ structure is described by the trigonal symmetry, $R\bar{3}m$ $(00\gamma)0s$ superspace group with the following parameters: $a_s = 11.4935(11)$ Å, $c_s = 2.9986(7)$ Å, $q = 0.57161(15)$ c*, and $V_s = 343.05(15)$ Å^3.

1. INTRODUCTION

In recent years the commensurate and incommensurate hexagonal perovskite oxides Sr_xMO_3 (M = Co, Ni, Cu, Zn, Ir, Pt) have received much attention due to the discovery of interesting magnetic properties (1, 2). The structures of these oxides are usually described as a stacking of mixed $[Sr_3O_9]$ and $[Sr_3MO_6]$ layers with the transition metal atoms M occupying the octahedral and trigonal prismatic sites (3, 4). Alternatively, they can be regarded as consisting of $(MO_3)_\infty$ and $(Sr)_\infty$ chains running parallel to each other (Fig. 1) (5). The $(MO_3)_\infty$ chains of Sr_xMO_3 are made up of face-sharing MO_6 octahedra and MO_6 trigonal prisms, in which the ordering and the ratio of the octahedra and trigonal prisms depend on the element M and on the value of x. Thus the perovskite oxides Sr_xMO_3 present diverse chemical compositions and physical properties (6). So far analogous sulfides Sr_xMS_3 are limited in number and their structures have not been fully characterized (7–9). The first complete structural determination of such sulfides was provided by a recent single crystal X-ray diffraction study of $Sr_{9/8}TiS_3$ (10) using the (3 + 1)-dimensional formalism (11). The crystal structure of $Sr_{8/7}TiS_3$ was similarly determined (12). The sulfides Sr_xMS_3 differ in structure somewhat from the hexagonal oxide perovskites Sr_xMO_3 in that the $(TiS_3)_\infty$ chains are made up of face-sharing octahedral (Oh) and polyhedral (PO) TiS_6 units. (Here a PO TiS_6 unit is obtained from a regular TiS_6 trigonal prism by rotating the two S_3 triangles around the three fold axis to make a dihedral angle of $\sim 30°$.) Both $Sr_{9/8}TiS_3$ and $Sr_{8/7}TiS_3$ have three $(TiS_3)_\infty$ chains per unit cell. All the $(TiS_3)_\infty$ chains of $Sr_{9/8}TiS_3$ have the $[-(PO-Oh-PO)-(Oh)_5-]_2$ repeat pattern (Fig. 2a). In contrast, $Sr_{8/7}TiS_3$ contains two kinds of $(MS_3)_\infty$ chains; i.e., its unit cell has one chain of the repeat pattern $[-(PO-PO)-(Oh)_5-]$ (Fig. 2b) and two chains of the repeat pattern $[-(Oh)_4-(PO-Oh-PO)-]$ (Fig. 2c).

In the $(TiS_3)_\infty$ chains of $Sr_{9/8}TiS_3$ and $Sr_{8/7}TiS_3$, the nearest-neighbor Ti–Ti distances within the $(Oh)_n$ ($n = 4, 5$) octahedral oligomers are short (< 3.0 Å) compared with all other nearest-neighbor Ti–Ti distances (> 3.0 Å). Moreover, within each $(Oh)_n$ group, the Ti–Ti distance becomes shorter as it moves closer to the center (see Section 4). It is

[1]To whom correspondence should be addressed.

0022-4596/01 $35.00

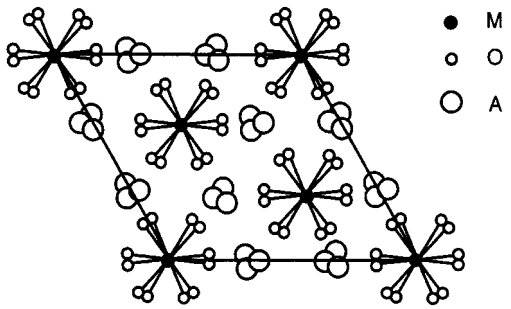

FIG. 1. Schematic projection view of the structure of a hexagonal perovskite-type compound A_xMO_3 along the $(MO_3)_\infty$ chain direction.

important to examine how these observations are related to the *d*-electron counts of $Sr_{9/8}TiS_3$ and $Sr_{8/7}TiS_3$. There are two *d*-electrons per $Sr_9(TiS_3)_8$ unit in $Sr_{9/8}TiS_3$, and two *d*-electrons per $Sr_8(TiS_3)_7$ unit in $Sr_{8/7}TiS_3$. This indicates that there are two *d*-electrons in each repeat pattern of the $(TiS_3)_\infty$ chains, namely, [(PO–Oh–PO)–$(Oh)_5$] of $Sr_{9/8}TiS_3$ as well as [(PO–PO)–$(Oh)_5$] and [$(Oh)_4$–(PO–Oh–PO)] of $Sr_{8/7}TiS_3$. Consequently, for each $(TiS_3)_\infty$ chain, only the lowest-lying *d*-block band should be filled. If we take the *z* axis along the $(TiS_3)_\infty$ chain direction, the z^2 orbitals of the Ti atoms in each $(Oh)_n$ oligomer should have significant sigma-type orbital interactions through the shared faces due to their short Ti–Ti distances. Therefore, the primary contributor to the lowest-lying *d*-block band of each $(TiS_3)_\infty$ chain should be the most sigma-bonding level of each $(Oh)_n$ oligomer constructed from its n z^2 orbitals. This gives rise to an "*n*-orbital two-electron bonding." (To a first approximation, the sigma-type orbital interactions involving the Ti–Ti bonds between PO and Oh units can be neglected due to their long Ti–Ti distances.) In the most bonding molecular orbital of a linear homoatomic molecule, all nearest-neighbor atoms have bonding interactions and the orbital contribution of each atom increases as it comes closer to the molecular center (13), so the strength of a nearest-neighbor bonding should become stronger as it moves toward the molecular center. Then the observed trends in the Ti–Ti distances of $Sr_{9/8}TiS_3$ and $Sr_{8/7}TiS_3$ can be explained if the only occupied *d*-block levels of each $(TiS_3)_\infty$ chain are the most sigma-bonding level of each $(Oh)_n$ oligomer constructed from its n z^2 orbitals.

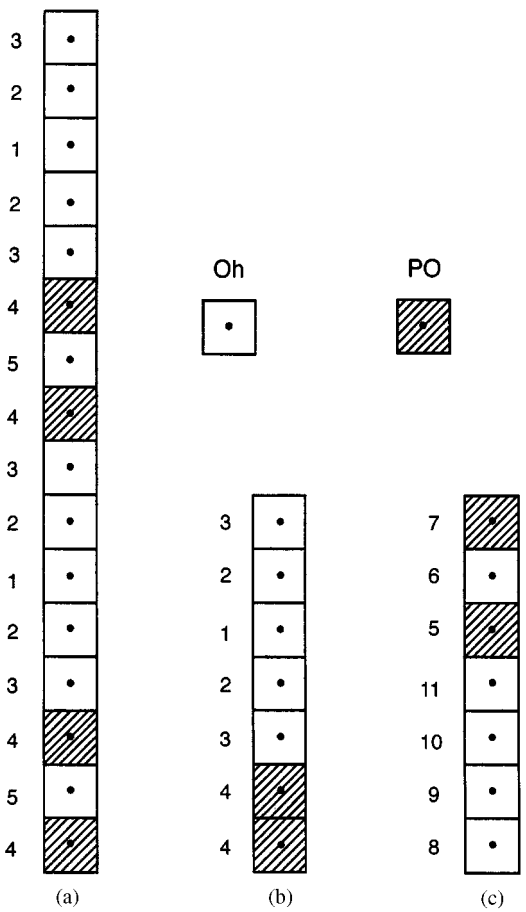

FIG. 2. Schematic representations of the repeat patterns of the TiS_6 octahedra and TiS_6 polyhedra in the $(TiS_3)_\infty$ chains of Sr_xTiS_3: (a) the $[-(PO-Oh-PO)-(Oh)_5-]_2$ chain of $Sr_{9/8}TiS_3$, (b) the $[-(PO-PO)-(Oh)_5-]$ chain of $Sr_{8/7}TiS_3$, and (c) the $[-(Oh)_4-(PO-Oh-PO)-]$ chain of $Sr_{8/7}TiS_3$, where each number *i* represents the Ti(*i*) atom.

To confirm the above prediction, we carry out electronic band structure calculations for $Sr_{9/8}TiS_3$ and $Sr_{8/7}TiS_3$ on the basis of the extended Hückel tight binding method (14, 15) using the atomic orbital parameters summarized in Table 1. There are two important questions associated with the concept of the *n*-orbital two-electron metal–metal sigma bonding. One is related to the *d*-orbital density distribution at the Ti sites in each $(TiS_3)_\infty$ chain. According to our discussion presented above, the Ti *d*-orbital density should be larger at the Oh sites of the $(Oh)_n$ oligomer than at any other sites, and this density in each $(Oh)_n$ oligomer should increase as the Ti atom moves closer to the oligomer center.

TABLE 1

Exponents ζ_i and Valence Shell Ionization Potentials H_{ii} of Slater-Type Orbitals χ_i Used for Extended Hückel Tight-Binding Calculations[a]

Atom	χ_i	H_{ii}(eV)	ζ_i	c_1[b]	$\zeta_{i'}$	c_2[b]
Ti	4*s*	− 8.97	1.500	1.0		
Ti	4*p*	− 5.44	1.500	1.0		
Ti	3*d*	− 10.8	4.550	0.4206	1.400	0.7839
S	2*s*	− 20.0	2.122	1.0		
S	2*p*	− 13.3	1.827	1.0		

[a] H_{ii} values are the diagonal matrix elements $\langle\chi_i|H^{eff}|\chi_i\rangle$, where H^{eff} is the effective Hamiltonian. In our calculations of the off-diagonal matrix elements $H^{eff} = \langle\chi_i|H^{eff}|\chi_j\rangle$, the weighted formula was used. See Ref. (28).

[b] Contraction coefficients used in the double-zeta Slater-type orbital.

TABLE 2
Crystallographic Data for $Sr_{8/7}Ti_{6/7}Fe_{1/7}S_3$

(1) Physical, crystallographic and analytical data	
Formula	$Sr_{8/7}Ti_{6/7}Fe_{1/7}S_3$
Crystal color	Black
Molecular weight ($g \cdot mol^{-1}$)	245.33
Crystal system	Trigonal
Space group (t section)	$R\bar{3}m$ $(00\gamma)0s$ ($t = 0 \Rightarrow P\bar{3}$)
Temperature (K)	293
Cell parameters	875 reflections on IPDS
a (Å)	11.4935(11)
c (Å)	2.9986(7)
	$\mathbf{q} = 0.57161(15)\ \mathbf{c}^* \equiv 4/7\mathbf{c}^*$
V (Å^3)	343.05(15)
Z	3
Density (calc., $g \cdot cm^{-3}$)	3.561
Crystal description	Block
Crystal size (mm^3)	$\sim 0.10 \times 0.10 \times 0.08$
(2) Data collection	
Monochromator	Oriented graphite (002)
Radiation	MoK-$L_{2,3}$ ($\lambda = 0.71073$ Å)
Scan mode	ω
No. of measured reflections	24,912
hkl range	$-12 < h < 12$
	$-13 < k < 13$
	$-23 < l < 23$
$\sin(\theta)/\lambda$ range (Å^{-1})	0–0.57
(3) Data reduction	
Linear absorption coeff. (cm^{-1})	164.2
Absorption correction	Analytical
T_{min}/T_{max}	0.31/0.42
No. of independent reflections	2467
Criterions for observed reflections	$I > 2\sigma(I)$
R_{int} (obs)	0.10
No. of observed reflections	1231
(4) Refinement	
Refinement	F^2
$F(000)$	338
Twin matrices	$\begin{pmatrix}1&0&0\\0&1&0\\0&0&1\end{pmatrix}, \begin{pmatrix}0&-1&0\\-1&0&0\\0&0&1\end{pmatrix}$
Twin fractions (%)	0.497(4), 0.503(4)
No. of reflections used in the refinement	2467
R (obs)[a]	4.34
R_w (obs)[a]	7.81
R (all)[a]	9.96
R_w (all)[a]	8.92
S	0.91
No. of refined parameters	100
Weighting scheme	$w = 1/(\sigma^2(I) + (2*0.016*I)^2)$
Difference Fourier residues	$[-1.7, +2.1] e^-/Å^3$

[a] $R = \sum \|F_o| - |F_c\| / \sum |F_o|$. $R_w = [\sum w(|F_o|^2 - |F_c|^2)^2 / \sum w|F_o|^4]^{1/2}$.

Then the idea of electronegativity perturbation (13) suggests that if a more electronegative transition metal cation (hence carrying a nonzero number of d-electrons) were to occupy the Ti sites of the $(TiS_3)_\infty$ chains, the more preferred site is one that has the larger z^2 orbital contribution in the lowest-lying d-block level, i.e., the Oh site of each $(Oh)_n$ oligomer closer to its center. To test this implication, we synthesized $Sr_{8/7}[Ti_{6/7}Fe_{1/7}]S_3$, an isostructural analogue of $Sr_{8/7}TiS_3$, and determined its crystal structure by single-crystal X-ray diffraction. Another important question is whether the bottom d-block band of each $(TiS_3)_\infty$ chain is separated from the rest of the d-block bands of the $(TiS_3)_\infty$ chain by a band gap. If so, the Sr_xMS_3 systems would be normal semiconductors. In the present work, we probe this question by measuring the temperature-dependent magnetic susceptibilities of $Sr_{9/8}TiS_3$, $Sr_{8/7}TiS_3$, and $Sr_{8/7}[Ti_{6/7}Fe_{1/7}]S_3$.

2. SYNTHESIS AND CRYSTAL STRUCTURE OF $Sr_{8/7}[Ti_{6/7}Fe_{1/7}]S_3$

Initially, single crystals of $Sr_{8/7}[Ti_{6/7}Fe_{1/7}]S_3$ were prepared from a mixture of the elements in the ratio Sr:Ti:Fe:S = 1.2:0.9:0.1:3 (Sr metal less than 6-mm pieces, 99.95%, Cerac; Ti sponge powders, 99.9%, Cerac; Fe powder, 99.9%, Alfa; S powder, >99.999%, Fluka), placed in a sealed, evacuated silica tube at 723 K for 2 days, and subsequently heated at 1273 K for 5 days. After natural cooling of the closed furnace, the product was ground for homogenization and reheated for crystallization again at 1273 K for 4 days. Samples of small blocks with a metallic luster were then obtained. The EDXS analysis of polished surfaces gave a formula close to $Sr_{1.15}Ti_{0.85}Fe_{0.15}S_3$. Later, a higher yield of $Sr_{8/7}[Ti_{6/7}Fe_{1/7}]S_3$ was obtained from a synthesis with a mixture of elements in stoichiometric ratio.

$Sr_{8/7}[Ti_{6/7}Fe_{1/7}]S_3$ single crystals were tested for quality (intensity and shape of the spots) on a Stoe image plate diffraction system (IPDS). The best crystal was selected for the data collection. The intensity measurement was carried out on the Stoe IPDS diffractometer in a medium-range resolution mode (plate at 80 mm, limiting $\sin(\theta)/\lambda$ to 0.57 Å^{-1}, 5 min exposure time). The reflection set was consistent with a trigonal symmetry and a metric that could be described in a hexagonal Bravais P-centered lattice ($a \approx 11.5$ Å and $c \approx 21.0$ Å). Since this reflection set is similar to that of $Sr_{8/7}TiS_3$ (12), we considered a modulated composite character of the structure with two sublattices and satellite reflections. (A detailed description of the concept of the $(3 + n)$-dimensional crystallography is given in the review papers by Janssen *et al.* (16) and van Smaalen (17).) The lattice parameters were least-squares refined using the (3 + 1)-D indexing formalism (18) from the positions of 875 reflections to obtain $a_s = 11.4935(11)$ Å, $c_s = 2.9986(7)$ Å, $\mathbf{q} = 0.57161(15)\ \mathbf{c}^*$, and $V_s = 343.05(15)$ Å^3. Accordingly, the reflection set was indexed with four indices. The γ component of the $\mathbf{q}$ wave vector was refined within roughly three standard uncertainties of the rational value $4/7 \approx 0.5714$.

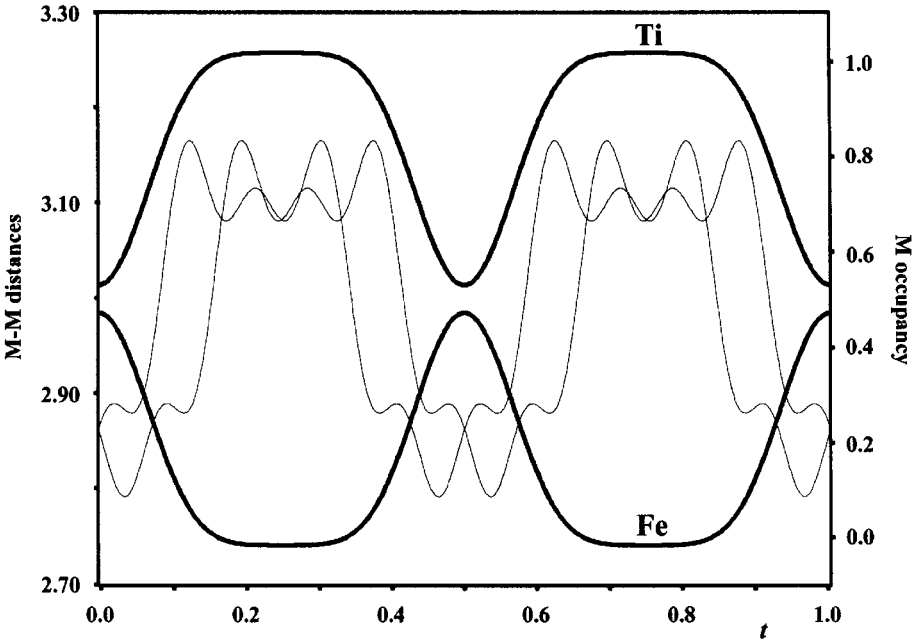

FIG. 3. Metal–metal distances along the $(MS_3)_\infty$ chains (thin lines, left) and metal site occupancy (think lines, right) as a function of the superspace internal coordinate t.

The intensities of the reflections collected for $Sr_{8/7}[Ti_{6/7}Fe_{1/7}]S_3$ were adjusted for Lorentz polarization and corrected for absorption via a Gaussian analytical method, and the crystal shape and dimensions were optimized with the Stoe X-Shape program (19) on the basis of equivalent reflections. All data treatments, refinements and Fourier syntheses were carried out with the Jana2000 program package (20). The redundant set of 24,912 reflections was averaged according to the $(\bar{3}m, \bar{1}1)$ (3 + 1)-D point group, yielding an internal R value of 0.10 for observed reflections ($I > 2\sigma(I)$) (see Table 2 for additional information). All refinements were performed on F^2 with all reflections included, but residual factors are thereafter reported for observed reflection only. As the starting point for the $Sr_{8/7}[Ti_{6/7}Fe_{1/7}]S_3$ structure refinements, we used the model established for $Sr_{8/7}TiS_3$ with crenel functions and twinning matrices (12). The advantages of using a (3 + 1)-D superspace approach for a commensurately modulated structure are (a) a possible reduction of the number of refined parameters that highly limit correlation (21) and (b) a unique description of phases that would otherwise have different space group and cell parameters for each composition (22–24).

In addition to the scheme employed for $Sr_{8/7}TiS_3$ in the setting of crenel functions, displacement and Debye–Waller factor modulation waves, and twinning matrices, we introduced a new occupation modulation function modeling the partial Ti/Fe substitution. The Fe atoms preferentially occupy the octahedral sites away from the PO sites. However, the Ti/Fe segregation was not abrupt and could not be modeled by a crenel function. The Ti and Fe occupations were therefore refined by means of Fourier waves up to the sixth order and constrained to a full site occupancy at any internal t coordinate, that is, for each Ti/Fe site of the real three-dimensional (3D) structure (see Fig. 3). A slight overshooting and undershooting of the occupation could not be avoided. In the final stage, the introduction of a twin law (already encountered for $Sr_{8/7}TiS_3$) led to the final residual value $R = 4.34\%$ ($R_w = 7.81\%$) for 100 parameters and 1231 observed reflections. Final refinement parameters for $Sr_{8/7}[Ti_{6/7}Fe_{1/7}]S_3$ are gathered in Table 2 and usual 3D atomic coordinates and displacement parameters are presented in Table 3. Note that no standard uncertainties could be given for the position and displacement parameters since a standard 3D refinement would require 169 parameters; that is, all parameters given in Table 3 are not independent.

The structure of $Sr_{8/7}Ti_{6/7}Fe_{1/7}S_3$ is quite similar to that of $Sr_{8/7}TiS_3$, which was described in detail in Ref. (12). Figure 4 shows that in each $(Ti_{6/7}Fe_{1/7}S_3)_\infty$ chain of $Sr_{8/7}[Ti_{6/7}Fe_{1/7}]S_3$ the Fe atoms favor the Ti sites of the $(Oh)_n$ oligomers over any other sites, and that in each $(Oh)_n$ oligomer the Fe atom prefers the Ti site closer to the oligomer center. These observations are precisely what were expected from the consideration of n-orbital two-electron metal–metal sigma bonding.

TABLE 3

Fractional Atomic Coordinates, Equivalent Isotropic Displacement Parameters (Å^2), and Site Occupancies for $Sr_{8/7}Ti_{6/7}Fe_{1/7}S_3$ (3D Supercell; Space Group $P\bar{3}$; Cell Parameters, $a = 11.4935(11)$ Å, $c = 20.990(5)$ Å)

Atom	x	y	z	U_{eq}	τ
Sr1	0.3158	0.3354	0.1881	0.025	1
Sr2	0.3618	0.3618	0.4360	0.022	1
Sr3	0.3321	0.3018	0.6794	0.024	1
Sr4	0.3342	0.3022	0.9428	0.020	1
Ti1	0	0	0	0.014	0.53
Fe1	0	0	0	0.014	0.47
Ti2	0	0	0.1364	0.013	0.74
Fe2	0	0	0.1364	0.013	0.26
Ti3	0	0	0.2764	0.012	0.98
Fe3	0	0	0.2764	0.012	0.02
Ti4	0	0	0.4258	0.014	1
Ti5	$\frac{2}{3}$	$\frac{1}{3}$	0.0444	0.013	1
Ti6	$\frac{2}{3}$	$\frac{1}{3}$	0.1918	0.014	1
Ti7	$\frac{2}{3}$	$\frac{1}{3}$	0.3388	0.013	1
Ti8	$\frac{2}{3}$	$\frac{1}{3}$	0.4852	0.012	0.85
Fe8	$\frac{2}{3}$	$\frac{1}{3}$	0.4852	0.012	0.15
Ti9	$\frac{2}{3}$	$\frac{1}{3}$	0.6229	0.014	0.56
Fe9	$\frac{2}{3}$	$\frac{1}{3}$	0.6229	0.014	0.44
Ti10	$\frac{2}{3}$	$\frac{1}{3}$	0.7565	0.013	0.64
Fe10	$\frac{2}{3}$	$\frac{1}{3}$	0.7565	0.013	0.36
Ti11	$\frac{2}{3}$	$\frac{1}{3}$	0.8937	0.012	0.93
Fe11	$\frac{2}{3}$	$\frac{1}{3}$	0.8937	0.012	0.07
S1	0.1857	0.1594	0.0682	0.011	1
S2	0.1673	−0.0023	0.2059	0.011	1
S3	0.1699	0.1587	0.3492	0.011	1
S4	0.0897	0.1849	0.5010	0.030	0.5
S5	0.5738	0.1454	0.1167	0.030	1
S6	0.7689	0.5212	0.2646	0.030	1
S7	0.4986	0.1674	0.4130	0.011	1
S8	0.8300	0.5113	0.5528	0.011	1
S9	0.5004	0.1530	0.6893	0.011	1
S10	0.8362	0.5022	0.8260	0.011	1
S11	0.5058	0.1635	0.9679	0.011	1

3. MAGNETIC PROPERTIES OF $Sr_{9/8}TiS_3$, $Sr_{8/7}TiS_3$, and $Sr_{8/7}[Ti_{6/7}Fe_{1/7}]S_3$

Static magnetic susceptibility measurements were carried out using a Quantum Design SQUID magnetometer and the ground samples of carefully selected crystals (283.1, 160.0, and 175.6 mg for $Sr_{9/8}TiS_3$, $Sr_{8/7}TiS_3$, and $Sr_{8/7}Ti_{6/7}Fe_{1/7}S_3$, respectively). An X-ray analysis of these samples did not reveal any impurity phases.

Magnetic susceptibility data were recorded for $Sr_{9/8}TiS_3$, $Sr_{8/7}TiS_3$, and $Sr_{8/7}[Ti_{6/7}Fe_{1/7}]S_3$ in a magnetic field of 1 kG after zero-field cooling. Figures 5 and 6 show the susceptibility versus temperature (χ vs T) curves determined for $Sr_{9/8}TiS_3$ and $Sr_{8/7}[Ti_{6/7}Fe_{1/7}]S_3$. The χ vs T behavior of $Sr_{8/7}TiS_3$ is practically the same as that of $Sr_{9/8}TiS_3$ within the experimental uncertainties, and hence is not presented here. From magnetization measurements at different fields at low and high temperatures (5 and 300 K), it can be concluded that no ferromagnetic impurities were present.

For $Sr_{9/8}TiS_3$ and $Sr_{8/7}TiS_3$, the susceptibility curves can be fitted with the expression $\chi = \chi_0 + C/(T - \theta)$, where χ_0 accounts for a temperature-independent term (which includes the core diamagnetism contribution). For $Sr_{9/8}TiS_3$ and $Sr_{8/7}TiS_3$, the best fit yields $C \approx 0.005\ cm^3 \cdot K \cdot mol^{-1}$, $\theta \approx -2$ K, and $\chi_0 \approx 1.6 \times 10^{-5}\ cm^3 \cdot mol^{-1}$. The Curie constant C corresponds only to $\sim 1.3\%$ of an unpaired $S = \frac{1}{2}$ spin. Such a small spin density implies that the spins of $Sr_{9/8}TiS_3$ and $Sr_{8/7}TiS_3$ originate from random structural defects of their $(TiS_3)_\infty$ chains. The χ_0 term is smaller than the absolute value of the estimated core diamagnetism contribution $\chi_{dia}(\approx -10^{-4}\ cm^3 \cdot mol^{-1})$. Thus, the value of χ at high temperature would be essentially due to a temperature-independent paramagnetism. This is expected for a semiconductor with a narrow conduction band of a predominantly metal d character. This finding indicates that in $Sr_{9/8}TiS_3$ and $Sr_{8/7}TiS_3$ the bottom d-block band of each $(TiS_3)_\infty$ chain is separated from the rest of the d-block bands by a small band gap.

The $\chi(T)$ curve for the powdered samples of $Sr_{8/7}[Ti_{6/7}Fe_{1/7}]S_3$ can also be fitted by the $\chi = \chi_0 + C/(T - \theta)$ formula with $\chi_0 = 7.5 \times 10^{-4}\ cm^3 \cdot mol$, $C = 3.1\ cm^3 \cdot K \cdot mol^{-1}$, and $\theta = -11.5$ K. The experimental magnetic moment of 4.96 μ_B/Fe agrees perfectly with a d^6 high-spin configuration of Fe^{2+} ($\mu_{theo.} = 4.90\ \mu_B$/Fe). Thus the charge balance of $Sr_{8/7}[Ti_{6/7}Fe_{1/7}]S_3$ can be written as $(Sr^{2+})_8(Ti^{4+})_6(Fe^{2+})(S^{2-})_{21}$. This means that d-electrons are present only at the Fe sites. The low Weiss constant $\theta = -11.5$ K suggests that there is a weak antiferromagnetic interaction between high-spin Fe^{2+} cations when they are located at adjacent Oh sites of the $(Oh)_n$ oligomers.

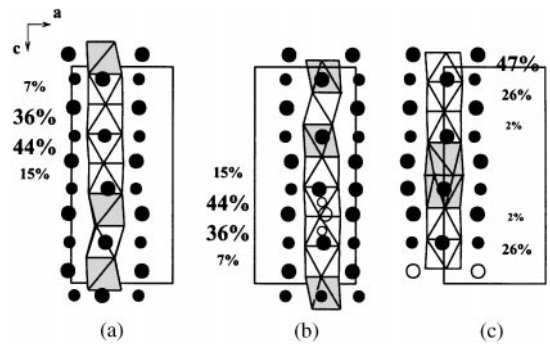

FIG. 4. Distribution of the Fe atoms in the Oh (unshaded) the PO (shaded) sites of the $(MS_3)_\infty$ chains of $Sr_{8/7}Ti_{6/7}Fe_{1/7}S_3$. The circles represent Sr atoms.

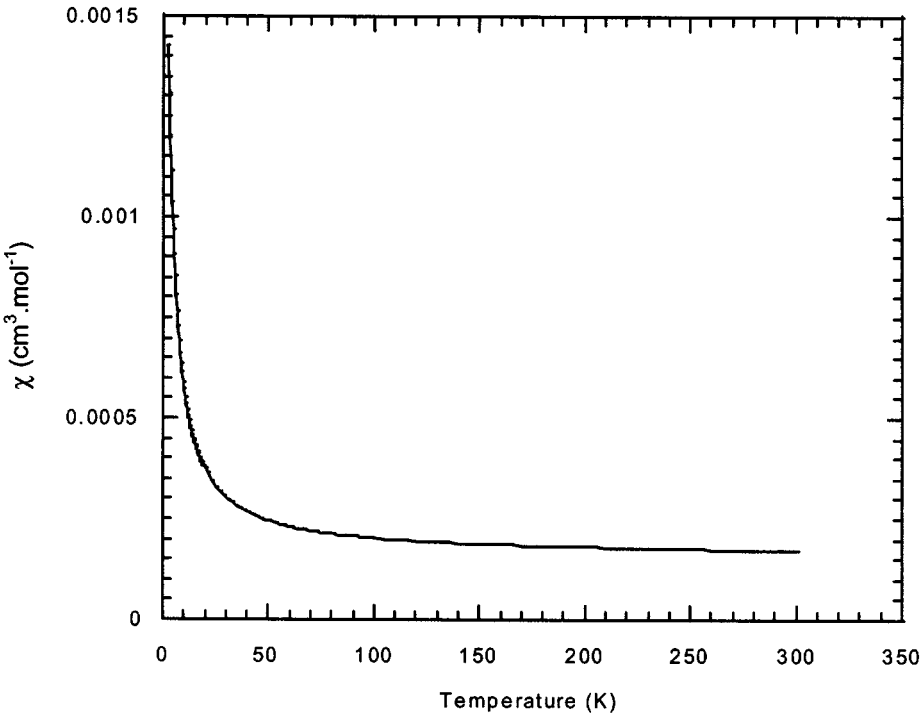

FIG. 5. Temperature dependence of the magnetic susceptibility of $Sr_{9/8}TiS_3$ measured in a magnetic field of 1 kG after a zero-field cooling.

4. Ti–Ti DISTANCES AND BOND VALENCE SUMS OF Ti

The nearest-neighbor Ti–Ti distances of the $(TiS_3)_\infty$ chains in $Sr_{9/8}TiS_3$ and $Sr_{8/7}TiS_3$ are summarized in Table 4. Also listed is the Ti–Ti distance of $BaTiS_3$, which has $(TiS_3)_\infty$ chains made up of only face-sharing TiS_6 octahedra. The trends in the Ti–Ti distances of $Sr_{8/7}TiS_3$ and $Sr_{9/8}TiS_3$ are similar. Namely, the Ti–Ti distances within

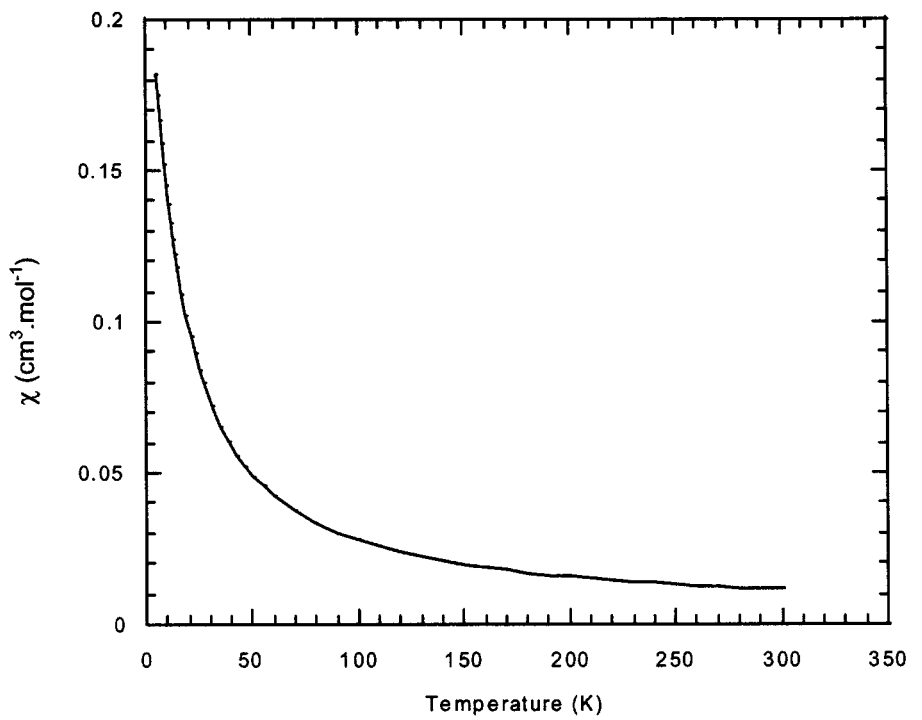

FIG. 6. Temperature dependence of the magnetic susceptibility of $Sr_{8/7}TiS_3$ measured in a magnetic field of 1 kG after a zero-field cooling.

TABLE 4
Nearest-Neighbor Ti–Ti Distances (Å) in the $(TiS_3)_\infty$ Chains of $Sr_{9/8}TiS_3$, $Sr_{8/7}TiS_3$, $Sr_{8/7}Ti_{6/7}Fe_{1/7}S_3$, and $BaTiS_3$

$Sr_{9/8}TiS_3$	$Sr_{8/7}TiS_3$	$Sr_{8/7}[Ti_{6/7}Fe_{1/7}]S_3$	$BaTiS_3$
Ti(1)–Ti(2) = 2.799	Ti(1)–Ti(2) = 2.816	*M*(1)–*M*(2) = 2.851	Ti–Ti = 2.899
Ti(2)–Ti(3) = 2.907	Ti(2)–Ti(3) = 2.930	*M*(2)–*M*(3) = 2.948	
Ti(3)–Ti(4) = 3.149	Ti(3)–Ti(4) = 3.163	*M*(3)–*M*(4) = 3.140	
Ti(4)–Ti(5) = 3.082	Ti(4)–Ti(4) = 3.140	*M*(4)–*M*(4) = 3.111	
	Ti(5)–Ti(6) = 3.095	*M*(5)–*M*(6) = 3.093	
	Ti(6)–Ti(7) = 3.094	*M*(6)–*M*(7) = 3.076	
	Ti(7)–Ti(8) = 3.108	*M*(7)–*M*(8) = 3.078	
	Ti(8)–Ti(9) = 2.885	*M*(8)–*M*(9) = 2.900	
	Ti(9)–Ti(10) = 2.782	*M*(9)–*M*(10) = 2.812	
	Ti(10)–Ti(11) = 2.844	*M*(10)–*M*(11) = 2.896	
	Ti(11)–Ti(5) = 3.150	*M*(11)–*M*(5) = 3.136	

the octahedral oligomer units $(Oh)_n$ ($n = 4, 5$) are shorter than any other Ti–Ti distances in the $(TiS_3)_\infty$ chains, and within each $(Oh)_n$ unit the closer the Ti–Ti distance is to its center, the shorter the distance is.

It is of interest to estimate the oxidation states of the Ti atoms of $Sr_{8/7}TiS_3$ and $Sr_{9/8}TiS_3$ by calculating their bond valence sum (BVS) values (25) on the basis of their Ti–S bond lengths. The oxidation state of Ti in $BaTiS_3$, which is $+4$ from the viewpoint of ionic electron counting, is calculated to be $+3.7$ according to the BVS analysis. Thus only the trend in the BVS values can be useful for our discussion. Our calculations reveal that within each $(Oh)_n$ ($n = 4, 5$) oligomer the BVS of Ti decreases, i.e., the *d*-electron density on Ti increases, as the Ti atom comes closer to the oligomer center. This is consistent with our conclusion that each $(Oh)_n$ oligomer unit of $Sr_{9/8}TiS_3$ and $Sr_{8/7}TiS_3$ has two *d*-electrons in its lowest-lying sigma bonding level derived from the z^2 orbitals. However, the BVS values of the PO site Ti atoms [i.e., Ti(4), Ti(5), and Ti(7)] are close to the lowest BVS values found for the $(Oh)_n$ oligomers. This is not consistent with our expectation that the *d*-electron densities should be greater for the Ti atoms of the $(Oh)_n$ oligomer units than for other Ti atoms. It should be recalled that the BVS analysis is unreliable when significant metal–metal bonding is present in a system (26) and also when bond lengths between two elements are significantly affected by the size of a third element in the structure (27). For each cases, a more reliable guide to electron counting and oxidation states is provided by electronic structure calculations, as will be discussed in the following.

5. ELECTRONIC BAND STRUCTURES OF $Sr_{9/8}TiS_3$ AND $Sr_{8/7}TiS_3$

Table 5 lists the values of the *d*-orbital gross populations calculated for the various Ti atoms of the $(TiS_3)_\infty$ chains in Sr_xTiS_3 ($x = 9/8, 8/7$). For the purpose of comparison, the corresponding value for the Ti atom of $BaTiS_3$ is also listed. For the $(TiS_3)_\infty$ chains of both $Sr_{9/8}TiS_3$ and $Sr_{8/7}TiS_3$, the *d*-electron density is higher for the Ti atoms of the $(Oh)_n$ oligomer than for other Ti atoms, and within each $(Oh)_n$ oligomer the closer the Ti atom is to the center of $(Oh)_n$, the higher its *d*-electron density (i.e., a lower oxidation state). Note that the preferential $Fe^{2+}(d^6)$ cation sites of $Sr_{8/7}[Ti_{6/7}Fe_{1/7}]S_3$ (i.e., the Ti(1), Ti(9), and Ti(10) sites) correspond to the Ti sites of $Sr_{8/7}TiS_3$ that provide a higher *d*-electron density. These results are in support of our expectations that the *d*-electron densities should be greater for the Ti atoms of the $(Oh)_n$ oligomer units than for other Ti atoms, and that within each $(Oh)_n$ ($n = 4, 5$) oligomer the *d*-electron density on Ti increases as the Ti atom comes closer to the oligomer center.

Figure 7a shows the dispersion relations of the bottom part of the *d*-block bands calculated for an isolated $(TiS_3)_\infty$ chain of $Sr_{9/8}TiS_3$. This chain has two $(Oh)_5$ oligomers per unit cell, i.e., four *d*-electrons per unit cell. Thus the bottom two bands are completely filled and are separated from the higher-lying bands by a band gap of 0.56 eV. The density of states (DOS) calculated for the chain shows that the filled *d*-block bands are largely composed of the Ti z^2 orbitals of the $(Oh)_5$ oligomer (Fig. 7b), and that the Ti z^2 orbital contribution to the filled *d*-block bands is larger for

TABLE 5
Values of the *d*-Orbital Gross Population (*Q*) Calculated for Each Ti Atom in the $(TiS_3)_\infty$ Chains of $Sr_{9/8}TiS_3$ and $Sr_{8/7}TiS_3$[a]

$Sr_{9/8}TiS_3$		$Sr_{8/7}TiS_3$				$BaTiS_3$	
Atom	*Q*	Atom	*Q*	Atom	*Q*	Atom	*Q*
Ti(1)	3.07	Ti(1)	3.08	Ti(5)	2.79	Ti(1)	2.60
Ti(2)	2.96	Ti(2)	2.96	Ti(6)	2.69		
Ti(3)	2.78	Ti(3)	2.77	Ti(7)	2.76		
Ti(4)	2.75	Ti(4)	2.76	Ti(8)	2.85		
Ti(5)	2.67			Ti(9)	3.06		
				Ti(10)	3.07		
				Ti(11)	2.87		

[a]The values of BVS and *Q* are in units of positive and negative unit changes, respectively.

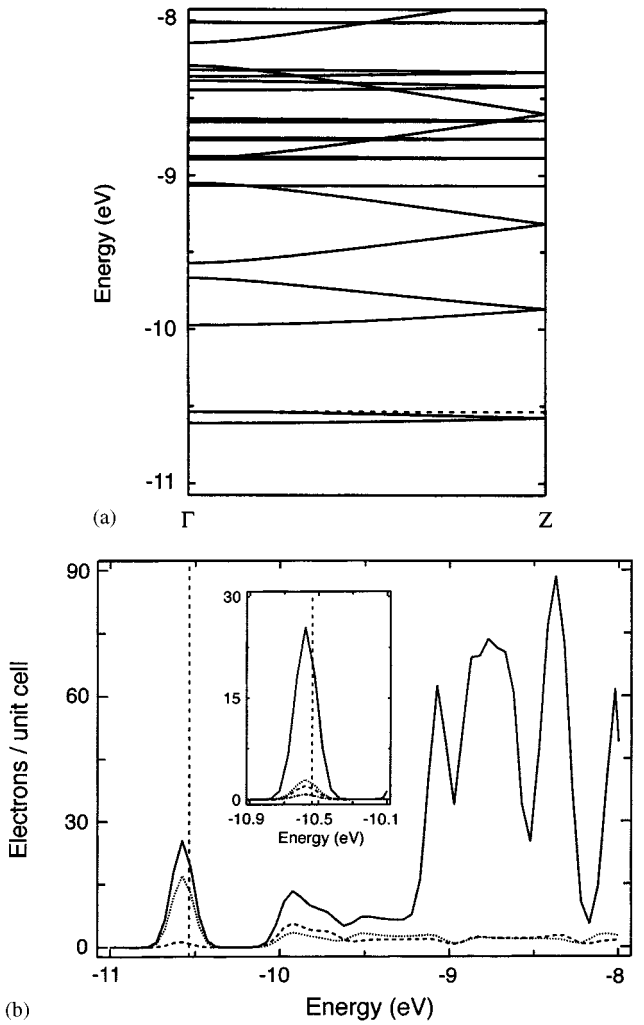

FIG. 7. Electronic band structure calculated for an isolated $(TiS_3)_\infty$ chain of $Sr_{9/8}TiS_3$: (a) the dispersion relations and (b) the density of states (DOS). In (b) the solid line represents the total DOS. The dotted line refers to the total z^2 orbital contributions from the Ti(1)–Ti(3) atoms, and the dashed line that from the Ti(4) and Ti(5) atoms. In the inset of (b) the dotted line refers to the z^2 orbital contribution from the Ti(1) atom, the dashed line that from the Ti(2) atom, and the dashed-dotted line that from the Ti(3) atoms. The Fermi level is presented as the horizontal dashed line in (a), and as the vertical dashed line in (b). The DOS curves in (b) exhibit small tails crossing the Fermi level. These artifacts arise from the Gaussian smoothing procedure used to obtain the DOS curves.

those Ti atoms closer to the oligomer center (i.e., Ti(1) > Ti(2) > Ti(3) in the inset of Fig. 7b). Similar trends are also found for $Sr_{8/7}TiS_3$. Figures 8a and 9a show the dispersion relations of the bottom part of the *d*-block bands calculated for the isolated $(TiS_3)_\infty$ chains that have the [–(PO–PO)–$(Oh)_5$–] and [–$(Oh)_4$–(PO–Oh–PO)–] repeat patterns, respectively. These chains have their bottom band completely filled and separated from the higher-lying bands by a band gap of 0.53 and 0.56 eV, respectively. The filled *d*-block bands are largely composed of the Ti z^2 orbitals of the $(Oh)_5$ and $(Oh)_4$ oligomers (Figs. 8b and 9b), and the Ti z^2 orbital contribution to these bands is larger for those Ti atoms closer to the oligomer center (i.e., Ti(1) > Ti(2) > Ti(3) in the inset of Fig. 8b; Ti(9) ≈ Ti(10) > Ti(8) ≈ Ti(11) in the inset of Fig. 9b).

To examine how the band gaps of the $(TiS_3)_\infty$ chains might be affected by the interchain interactions, we carry out electronic band structure calculations for the 3D structures of $Sr_{9/8}TiS_3$ and $Sr_{8/7}TiS_3$. Figure 10a shows the dispersion relations of the bottom portion of the *d*-block bands calculated for $Sr_{9/8}TiS_3$, and Fig. 10b

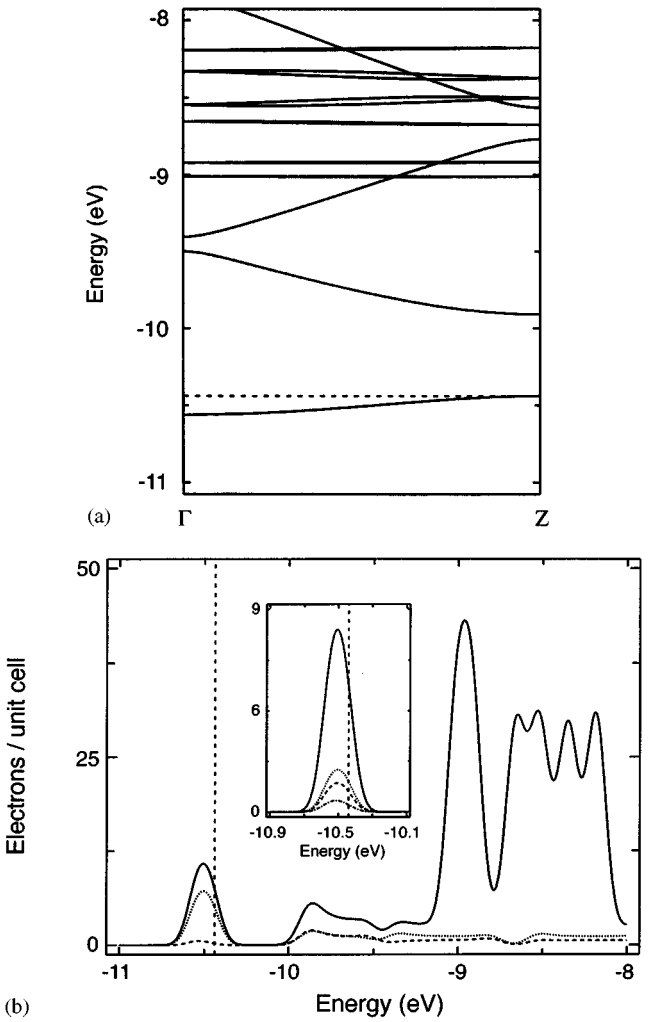

FIG. 8. Electronic band structure calculated for an isolated $(TiS_3)_\infty$ chain of $Sr_{8/7}TiS_3$ containing the Ti(1)–Ti(4) atoms: (a) the dispersion relations and (b) the density of states. In (b) the solid line represents the total density of states. The dotted line refers to the total z^2 orbital contributions from the Ti(1)–Ti(3) atoms, and the dashed line that from the Ti(4) atoms. In the inset of (b) the dotted line refers to the z^2 orbital contribution from the Ti(1) atom, the dashed line that from the Ti(2) atom, and the dashed-dotted line that from the Ti(3) atoms. The Fermi level is presented as the horizontal dashed line in (a), and as the vertical dashed line in (b). The DOS curves in (b) exhibit small tails crossing the Fermi level. These artifacts arise from the Gaussian smoothing procedure used to obtain the DOS curves.

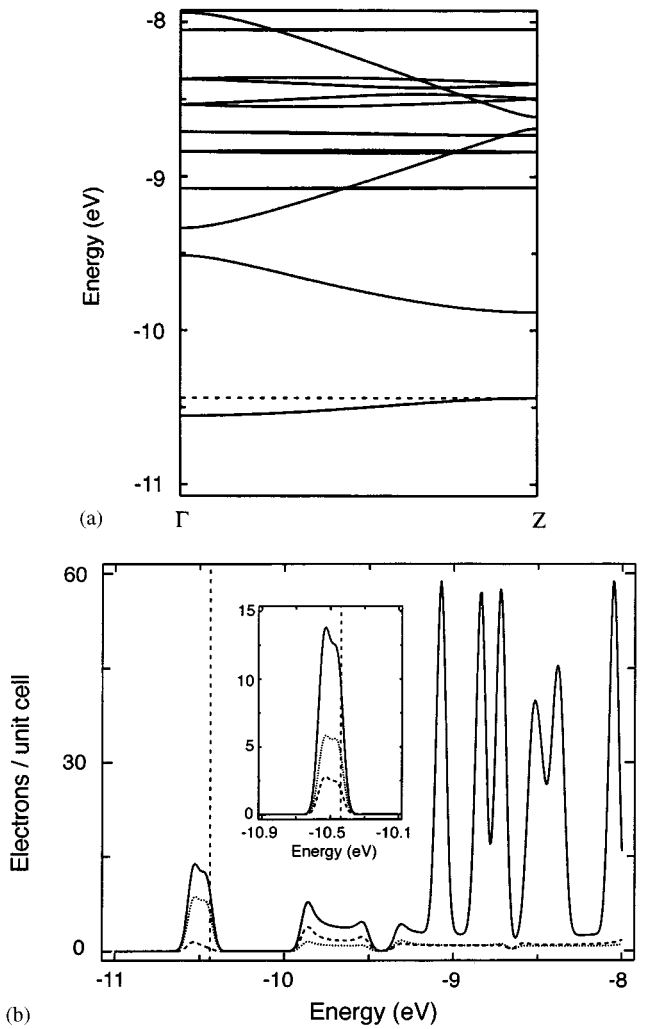

FIG. 9. Electronic band structure calculated for an isolated $(TiS_3)_\infty$ chain of $Sr_{8/7}TiS_3$ containing the Ti(5)–Ti(11) atoms: (a) the dispersion relations and (b) the density of states. In (b) the solid line represents the total density of states. The dotted line refers to the total z^2 orbital contributions from the Ti(8)–Ti(11) atoms, and the dashed line those from the Ti(5)–Ti(7) atoms. In the inset of (b) the dotted line refers to the z^2 orbital contributions from the Ti(9) and Ti(10) atoms, the dashed line those from the Ti(8) and Ti(11) atoms. The Fermi level is presented as the horizontal dashed line in (a), and as the vertical dashed line in (b). The DOS curves in (b) exhibit small tails crossing the Fermi level. These artifacts arise from the Gaussian smoothing procedure used to obtain the DOS curves.

those for $Sr_{8/7}TiS_3$. The band gap is calculated to be 0.32 eV in $Sr_{9/8}TiS_3$, and 0.29 eV in $Sr_{8/7}TiS_3$. Thus from the viewpoint of the electronic structures of isolated $(TiS_3)_\infty$ chains, the interchain interactions in $Sr_{9/8}TiS_3$ and $Sr_{8/7}TiS_3$ reduce the band gap. The presence of a small band gap in $Sr_{9/8}TiS_3$ and $Sr_{8/7}TiS_3$ is consistent with our experimental observations that $Sr_{9/8}TiS_3$ and $Sr_{8/7}TiS_3$ are diamagnetic, and that the magnetic susceptibility exhibits a preponderant temperature-independent paramagnetism at high temperature.

6. CONCLUDING REMARKS

The analysis of the trends in the nearest-neighbor Ti–Ti distances of the $(TiS_3)_\infty$ chains of $Sr_{9/8}TiS_3$ and $Sr_{8/7}TiS_3$ predicts that the occupied d-block band of each $(TiS_3)_\infty$ chain is the lowest-lying z^2 orbital band, and this band is mainly composed of the n-orbital two-electron metal–metal sigma bonding level of each oligomer $(Oh)_n$. These predictions are supported by electronic band structure calculations for $Sr_{9/8}TiS_3$ and $Sr_{8/7}TiS_3$. The n-orbital two-electron bonding picture implies that if the Ti sites of the $(TiS_3)_\infty$ chains were to be doped by a more electronegative transition metal cation, the preferred doping sites should be the Oh sites of the $(Oh)_n$ oligomers closer to their centers.

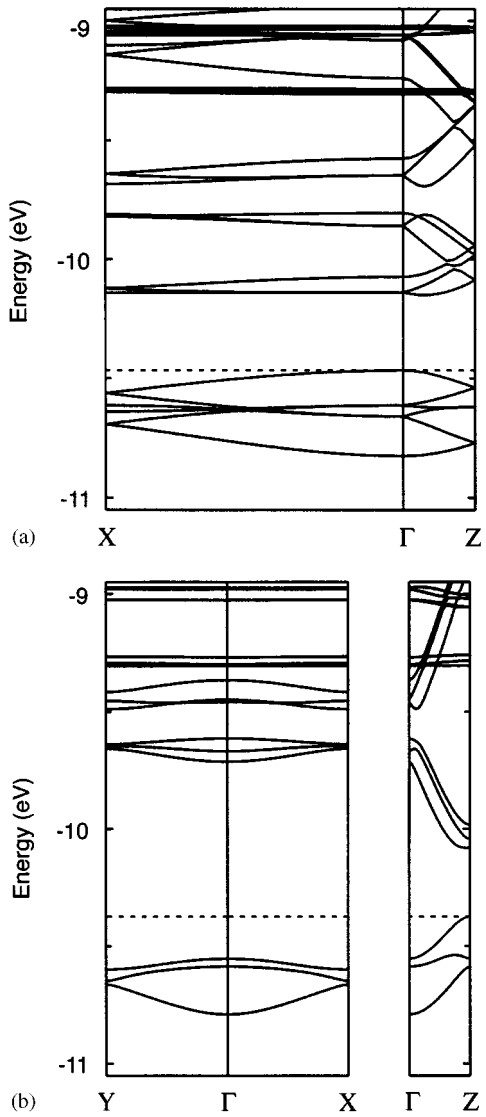

FIG. 10. Dispersion relations of the bottom part of the d-block bands calculated for the 3D structures of Sr_xTiS_3: (a) $Sr_{9/8}TiS_3$ and (b) $Sr_{8/7}TiS_3$. The Fermi level is presented as the horizontal dashed line in (a) and (b).

This implication was verified by synthesizing $Sr_{8/7}[Ti_{6/7}Fe_{1/7}]S_3$ and solving its crystal structure. Both the magnetic susceptibility measurements and electronic band structure calculations show that $Sr_{9/8}TiS_3$ and $Sr_{8/7}TiS_3$ are normal semiconductors in which the valence and conduction bands are separated by a small band gap. The magnetic susceptibility measurements for $Sr_{8/7}[Ti_{6/7}Fe_{1/7}]S_3$ indicate that it has Fe^{2+} (d^6) cations in high-spin configuration.

ACKNOWLEDGMENTS

Work at North Carolina State University was supported by the Office of Basic Energy Sciences, Division of Materials Science, U.S. Department of Energy, under Grant DE-FG05-86ER45259. The authors thank Professor C. Payen for helpful discussions on the magnetic properties of $Sr_{9/8}TiS_3$ and $Sr_{8/7}TiS_3$.

REFERENCES

1. T. N. Nguyen and H.-C. zur Loye, *J Solid State Chem.* **117,** 300 (1995).
2. T. N. Nguyen, P. A. Lee and H.-C. zur Loye, *Science* **271,** 489 (1996).
3. J. Darriet and M. A. Subramanian, *J. Mater. Chem.* **5,** 543 (1995).
4. C. Dussarat, F. Grasset, and J. Darriet, *Eur. J. Solid State Inorg. Chem.* **32,** 557 (1995).
5. K. Ukei, A. Yamamoto, Y. Watanabe, T. Shishido, and T. Fukuda, *Acta Crystallogr. Sect. B* **49,** 67 (1993).
6. M.-H. Whangbo, H.-J. Koo, K.-S. Lee, O. Gourdon, M. Evain, S. Jobic, and R. Brec, *J. Solid State Chem.* **160,** 239 (2001).
7. M. Saeki and M. Onoda, *J. Solid State Chem.* **102,** 100 (1993).
8. M. Saeki and M. Onoda, *J. Solid State Chem.* **112,** 65 (1994).
9. M. Onoda, M. Saeki, A. Yamamoto, and K. Kato, *Acta Crystallogr. Sect. B* **49,** 929 (1993).
10. O. Gourdon, V. Petricek, and M. Evain, *Acta Crystallogr. Sect. B* **56,** 409 (2000).
11. S. van Smaalen, *Crystallogr. Rev.* **4,** 79 (1995).
12. O. Gourdon, L. Cario, V. Petricek, J. M. Perez-Mato, and M. Evain, *Z. Kristallogr.*, in press.
13. T. A. Albright, J. K. Burdett, M.-H. Whangbo, "Orbital Interactions in Chemistry," Wiley, New York, 1985.
14. M.-H. Whangbo and R. Hoffmann, *J. Am. Chem. Soc.* **100,** 6093 (1978).
15. Our calculations were carried out by employing the CAESAR program package (J. Ren, W. Liang and M.-H. Whangbo, "Crystal and Electronic Structure Analysis Using CAESAR," 1998, available at http://www.PrimeC.com/).
16. T. Janssen, A. Janner, A. Looijenga-Vos, and P. M. de Wolff, *in* "International Tables for X-Ray Crystallography, Vol. C, Mathematical, Physical and Chemical Tables" (A. J. C. Wilson, Ed.), Chap. 9.8, Kluwer Academic, Dordrecht, 1993.
17. S. van Smaalen, *Crystallogr. Rev.* **4,** 79 (1995).
18. M. Evain, U-Fit program, Institut des Matériaux Jean Rouxel, Nantes, 1992.
19. Stoe, X-Shape program, Stoe & Cie Gmbh, Darmstadt, Germany, 1996.
20. V. Petricek and M. Dusek, JANA2000 program, Institute of Physics, Academy of Sciences of the Czech Republic, Prague, 2000.
21. J. M. Perez-Mato, *in* "Superspace Description of Commensurately Structures and Quasicrystals (J. M. Perez-Mato, F. J. Zunig, and G. Madariaga, Eds.), p. 117, World Scientific, Singapore, 1991.
22. M. Evain, F. Boucher, O. Gourdon, V. Petricek, M. Dusek, and P. Bezdicka, *Chem. Mater.* **10,** 3068 (1998).
23. J. M. Perez-Mato, M. Zakhour-Nakhl, F. Weill, and J. Darriet, *J. Mater. Chem.* **9,** 2795 (1999).
24. O. Gourdon, V. Petricek, M. Dusek, P. Bezdicka, S. Durovic, D. Gyepesova, and M. Evain, *Acta Crystallogr. B* **55,** 841 (1999).
25. I. D. Brown and D. Altermatt, *Acta Crystallogr. B* **41,** 244 (1985).
26. S. Wang, S.-J. Hwu, J. A. Paradis, and M.-H. Whangbo, *J. Am. Chem. Soc.* **117,** 5515 (1995).
27. M.-H. Whangbo and C. C. Torardi, *Science* **249,** 1143 (1990).
28. J. Ammeter, H.-B. Bürgi, J. Thibeautt, and R. Hoffman, *J. Am. Chem. Soc.* **100,** 3686 (1978).